AGU PUBLICATIONS

JGR

Journal of Geophysical Research: Atmospheres

RESEARCH ARTICLE
10.1002/2016JD025943

Key Points:
- Freezing level heights indicate a close link to glacier extents via the snow/rain transition height, albedo, and net shortwave radiation
- CMIP5 projections reveal that by the end of the 21st century, the freezing level height will rise by 230 m (850 m) for RCP2.6 (RCP8.5)
- By the end of this century, glaciers may shrink considerably under RCP2.6 and only remain at the highest summits under RCP8.5

Supporting Information:
- Supporting Information S1

Correspondence to:
S. Schauwecker,
schauwecker@meteodat.ch

Citation:
Schauwecker, S., M. Rohrer, C. Huggel, J. Endries, N. Montoya, R. Neukom, B. Perry, N. Salzmann, M. Schwarb, and W. Suarez (2017), The freezing level in the tropical Andes, Peru: An indicator for present and future glacier extents, *J. Geophys. Res. Atmos.*, *122*, doi:10.1002/2016JD025943.

Received 16 SEP 2016
Accepted 26 APR 2017
Accepted article online 28 APR 2017

The freezing level in the tropical Andes, Peru: An indicator for present and future glacier extents

Simone Schauwecker[1,2], Mario Rohrer[1], Christian Huggel[2], Jason Endries[3], Nilton Montoya[4], Raphael Neukom[5], Baker Perry[3], Nadine Salzmann[6], Manfred Schwarb[1], and Wilson Suarez[7]

[1]Meteodat GmbH, Zurich, Switzerland, [2]Department of Geography, University of Zurich, Zurich, Switzerland, [3]Department of Geography and Planning, Appalachian State University, Boone, North Carolina, USA, [4]Professional School of Agronomy, National University of San Antonio Abad at Cusco, Cusco, Peru, [5]Oeschger Centre for Climate Change Research and Institute of Geography, University of Bern, Bern, Switzerland, [6]Department of Geosciences, University of Fribourg, Fribourg, Switzerland, [7]Servicio Nacional de Meteorología e Hidrología del Perú SENAMHI, Lima, Peru

Abstract Along with air temperatures, the freezing level height (FLH) has risen over the last decades. The mass balance of tropical glaciers in Peru is highly sensitive to a rise in the FLH, mainly due to a decrease in accumulation and increase of energy for ablation caused by reduced albedo. Knowledge of future changes in the FLH is thus crucial to estimating changes in glacier extents. Since in situ data are scarce at altitudes where glaciers exist (above ~4800 m above sea level (asl)), reliable FLH estimates must be derived from multiple data types. Here we assessed the FLHs and their spatiotemporal variability, as well as the related snow/rain transition in the two largest glacier-covered regions in Peru by combining data from two climate reanalysis products, Tropical Rainfall Measuring Mission (TRMM) Precipitation Radar Bright Band data, Micro Rain Radar data, and meteorological ground station measurements. The mean annual FLH lies at 4900 and 5010 m asl, for the Cordillera Blanca and Vilcanota, respectively. During the wet season, the FLH in the Cordillera Vilcanota lies ~150 m higher compared to the Cordillera Blanca, which is in line with the higher glacier terminus elevations. Coupled Model Intercomparison Project version 5 (CMIP5) climate model projections reveal that by the end of the 21st century, the FLH will rise by 230 m (±190 m) for Representative Concentration Pathway (RCP) 2.6 and 850 m (±390 m) for RCP8.5. Even under the most optimistic scenario, glaciers may continue shrinking considerably, assuming a close relation between FLH and glacier extents. Under the most pessimistic scenario, glaciers may only remain at the highest summits above approximately 5800 m asl.

1. Introduction

Observations show that the retreat of glaciers in the 21st century is unprecedented on a global scale for the time period observed and probably also for the recorded history [*Zemp et al.*, 2015]. Glaciers play an important role in many regions in Peru, particularly because (1) there is a strong seasonality in precipitation with a considerable contribution of glacier melt to total river discharge during the dry season [e.g., *Kaser et al.*, 2003; *Mark et al.*, 2005; *Kaser et al.*, 2010]; (2) people use river water for irrigation, hydropower, tourism, or domestic consumption [e.g., *Drenkhan et al.*, 2015; *Gurgiser et al.*, 2016]; and (3) discharge from glaciers is expected to change in the future due to glacier shrinkage [*Ames and Hastenrath*, 1996; *Kaser and Georges*, 1997; *Mark and Seltzer*, 2003; *Juen et al.*, 2007; *Vuille et al.*, 2008; *Baraer et al.*, 2012; *Rabatel et al.*, 2013]. The consequences of vanishing glaciers are especially severe where people have only limited capacity to adapt to changes in the water availability due to, for instance, lack of financial resources and knowledge or/and where competition for water is intensifying [*Lynch*, 2012]. Various studies have shown that glaciers in Peru are rapidly shrinking since they are out of equilibrium with current climatic conditions [*Vuille et al.*, 2008; *Rabatel et al.*, 2013; *Salzmann et al.*, 2013]. Especially small glaciers at lower elevations will almost certainly disappear in a few years to decades [*Vuille et al.*, 2008; *Schauwecker et al.*, 2014]. Also, large glaciers with response times of 10–40 years [*Schauwecker et al.*, 2014] will continue retreating during the coming decades.

A crucial step to projecting future glacier shrinkage is understanding the dominant processes of glacier ablation and how these processes will change in future. Several studies have identified the net shortwave radiation budget as the main energy source for ablation of tropical glaciers [e.g., *Favier et al.*, 2004a, 2004b; *Gurgiser et al.*, 2013a, 2013b]. Net shortwave radiation is largely determined by albedo, which is strongly

affected by the snowline, the snowfall level height (SLH), and thereby the temperature during precipitation events [*Francou et al.*, 2004]. This close link between the air temperature during precipitation events, albedo and net shortwave radiation together with the fact that glacier tongues are constantly close to melting conditions, leads to a high sensitivity of tropical glaciers to air temperature which is described in several studies [e.g., *Kaser*, 2001; *Vuille et al.*, 2008; *Gurgiser et al.*, 2013a]. For example, *Gurgiser et al.* [2013a] showed that the glacier mass balance of the Shallap Glacier (Cordillera Blanca, Peru) varied significantly between 2 years due to different air temperatures and related SLHs, mainly during the wet season. While the mass balance in the accumulation area (>5000 m asl) was similar in both years due to similar annual total solid precipitation, the difference in mass balance was considerable for the lower part of the glaciers. *Gurgiser et al.* [2013a] suggest that the Shallap Glacier is characterized by a high sensitivity of mass balance to air temperature and is thus more similar to glaciers in the inner tropics (Ecuador) than the outer tropics (Bolivia) [*Favier et al.*, 2004a, 2004b].

The SLH (also called snow/rain transition height or melting level) is thus a crucial variable in accurately determining mass balance and runoff for tropical glaciers The SLH is defined as the top of the melting layer during precipitation events, which is the altitude throughout solid precipitation melts as it descends [*American Meteorological Society*, 2016]. The temperature of the melting layer is typically 0°C or warmer [*American Meteorological Society*, 2016]. The freezing level height (FLH, or also called freezing height or free air 0°C isotherm) is defined as the lowest level in the free atmosphere where the temperature is 0°C [*American Meteorological Society*, 2016]. Since melting of solid precipitation starts approximately where air temperature is over 0°C, the FLH during precipitation events and the SLH are closely related. It is thus crucial to study the seasonal and regional variabilities of the FLH, past and future changes, and how the FLH during precipitation events is linked to the SLH.

The FLH is on average within about 4500–5000 m asl in tropical regions between 20°N and 20°S [*Harris et al.*, 2000]. National Centers for Environmental Prediction/National Center for Atmospheric Research (NCEP/NCAR) reanalysis data show that over the last 30 years, the FLH has increased by 10–20 m per decade over the tropics (1977–2007 [*Bradley et al.*, 2009]) and by about 30 m per decade over the Cordillera Blanca (1960–2010 [*Rabatel et al.*, 2013]). Also, *Diaz et al.* [2003] found that the tropical (20°N–20°S) FLH increased by about 14 m per decade from 1948 to 2000 and by 12 m per decade between 1958 and 2000. In addition to reanalysis data, station data indicate that the FLH during precipitation days has risen by about 200 m during the five decades between the 1960s and 2012 in the Cordillera Blanca [*Schauwecker et al.*, 2014]. In the recent years, large efforts have been made to monitor air temperature and precipitation at high altitudes in order to assess the snow/rain transition and precipitation type [e.g., *Poremba et al.*, 2015]. However, meteorological measurements at the elevation of glaciers (>4800 m asl) are still very sparse and often limited to short time periods, thus limiting the estimation of the FLH and SLH. This calls for studies based on data from multiple sources, e.g., radiosondes, precipitation radar, reanalysis data, or remote sensing. The first objective of this article is therefore to assess the spatial and temporal variabilities of the FLH and the link to the SLH over the two largest glacierized mountain ranges in Peru, the Cordillera Blanca (CB; Figure 1), and the Cordillera Vilcanota (CV; Figure 1), using remote sensing, reanalysis, and in situ data.

Our second objective is to assess future FLHs by the end of this century, using global climate model (GCM) outputs. Model projections indicate a continued warming of the tropical troposphere throughout the 21st century, but, to our knowledge, the future FLH has not yet been assessed for the mountainous regions of Peru. GCMs driven by the Special Report on Emissions Scenarios (SRES) A2 indicate an increase in mean air temperature on the order of 4.5 to 5°C [*Bradley et al.*, 2006; *Vuille et al.*, 2008; *Urrutia and Vuille*, 2009] over Peru, whereas for B2 scenarios, a smaller warming of around 3 to 3.5°C results [*Urrutia and Vuille*, 2009]. *Bradley et al.* [2004, 2006] found that warming particularly affects high mountain regions and suggested that these changes could likely result in the complete disappearance of glaciers in many regions.

A third objective of this article is to discuss possible future glacier extents under different Representative Concentration Pathways (RCPs [*Moss et al.*, 2010]). While several studies have focused on future air temperature, little is known about future glacier extents in the Peruvian Cordilleras. For glaciers in High Asia, a rise of 10 m in summer FLH causes a strong decrease in mass balance and increase in the equilibrium line altitude (ELA) of up to 10 m [*Wang et al.*, 2014]. But, to our knowledge, this relationship has not been investigated for glaciers in Peru. Studies on the future of Peruvian glaciers have mostly been motivated

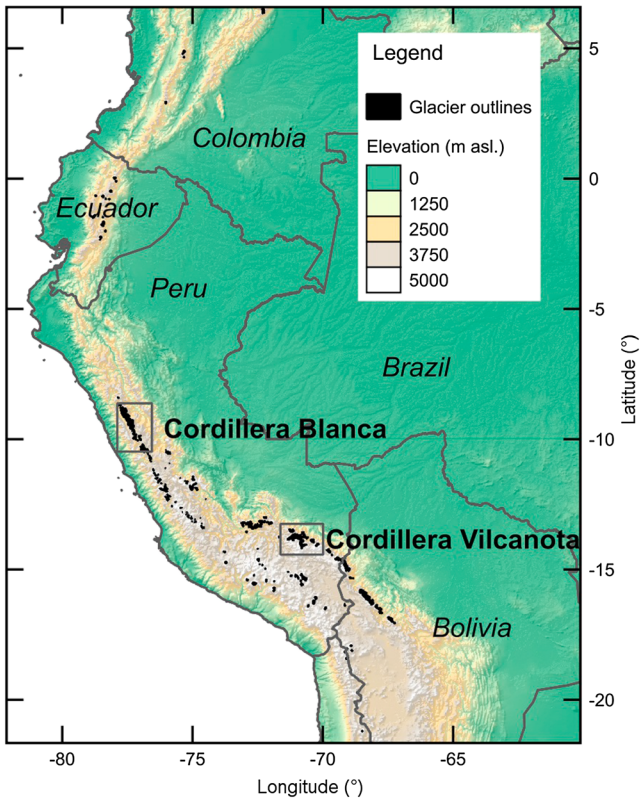

Figure 1. Overview map of the study areas CB and CV.

by future runoff from glaciated catchments [e.g., *Juen et al.*, 2007; *López-Moreno et al.*, 2014], but future glacier shrinkage and the response of tropical glaciers to temperature rise have still not been analyzed in detail nor fully understood. The glacier-climate interactions are complex because temperature not only affects the sensible heat flux but also influences other energy fluxes like incoming longwave radiation and net shortwave radiation via the SLH and albedo [see, e.g., *Vuille et al.*, 2008]. We discuss here the future glacier extents based on a simple experiment, assuming a strong and stable relation between the FLH during precipitation events, the closely connected SLH, and glacier extents (as already indicated by, e.g., *Rabatel et al.* [2013]).

2. Study Sites

In our study we focus on the two largest glacier-covered tropical mountain ranges in Peru (Figure 1): The CB (9.0°S/77.5°W) and the CV (13.7°S/71.0°W). The termini of glaciers are currently located at around 4200 to 4800 m asl in the CB [*Racoviteanu et al.*, 2008] and 4600 to maximum 5400 m asl in the CV [*Salzmann et al.*, 2013].

The climate of the Peruvian Cordilleras is characterized by a distinct dry and wet season, defined by the global circulation patterns of the Intertropical Convergence Zone and the trade winds. Station data from the Servicio Nacional de Meteorología e Hidrología de Perú (SENAMHI) indicate that over 90% of the precipitation in the CB falls during the wet season from October to April, but some precipitation also occurs during the dry season, especially at high elevations [*Schauwecker et al.*, 2014]. Precipitation events are predominantly graupel at the elevation of the glacier tongues in the CV [*Poremba et al.*, 2015], similar to other tropical high mountain regions in the world (e.g., on Mount Kenya [*Prinz et al.*, 2016]). Since the bulk of the moisture advection is coming from the tropical Atlantic and the Amazon basin, interannual precipitation correlates well with easterly winds of the upper troposphere [e.g., *Garreaud et al.*, 2003; *Minveille and Garreaud*, 2011; *Schauwecker et al.*, 2014; *Neukom et al.*, 2015]. In contrast to the strong seasonal variation in precipitation, the Peruvian Cordilleras are characterized by small seasonal temperature variability. During the dry season, the diurnal variation in air temperature is more pronounced and mean daily air temperatures are lower compared to the wet season [*Schauwecker et al.*, 2014].

Several studies show that the climate in the tropical Andes has changed significantly over the last century [*Vuille and Bradley*, 2000; *Mark and Seltzer*, 2005; *Vuille et al.*, 2008; *Schauwecker et al.*, 2014]. Air temperature trends between 1983 and 2012 in the CB were −0.04 and 0.29°C per decade for T_{min} and T_{max}, respectively [*Schauwecker et al.*, 2014]. Between 1980 and 2009, air temperature has changed in the CV by −0.2 and 0.23°C per decade for T_{min} and T_{max}, respectively [*Salzmann et al.*, 2013].

3. Data and Methods

Since in situ meteorological data are relatively sparse along the Peruvian Cordilleras and at high elevations in particular, we assessed FLHs and SLHs using a combination of multiple data sets. These data products have different temporal and spatial resolutions and coverages, as schematically shown in Figure 2. An overview of

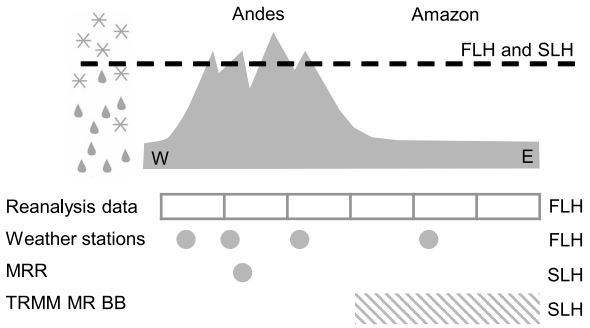

Figure 2. Schematic of the FLH and SLH over the Peruvian Cordillera from the West to the East and spatial availability of different data types, used for deriving SLH and FLH (indicated on the right). The boxes representing reanalysis data illustrate that the data are provided for a regular global grid. Weather stations and MRR data are available as point measurements. TRMM MR BB data are available for a variable spatial and temporal resolution, and limited over mountainous regions [e.g., *Schauwecker et al.*, 2016].

the data types is presented in Table 1. Reanalysis data are first used to assess seasonal and regional patterns in FLH over Peru. Furthermore, we compared reanalysis FLH as well as extrapolated FLH from the METAR station at the airport of Cusco to the SLH derived from the Micro Rain Radar (MRR). The SLH data derived by the MRR for all events are then compared to reanalysis data and to the extrapolated FLH. In addition, we estimated monthly FLH and SLH for all available data sets.

3.1. Reanalysis Data

Our study is based on two reanalysis products: ERA-Interim (interim reanalysis of the European Centre for Medium-Range Weather Forecasts (ECMWF)) [*Dee et al.*, 2011] and MERRA2 (reanalysis of the Modern Era Retrospective-Analysis for Research and Applications by the National Aeronautics and Space Administration (NASA)) [*Rienecker et al.*, 2011]. Large warm daily maximum air temperature biases of MERRA over southern America have largely been removed in MERRA2 [*Bosilovich et al.*, 2015]. *Hofer et al.* [2010] found that the skill of MERRA as predictor for daily air temperature on high altitudes in Peru is considerably higher than for other reanalysis products. Reanalysis data cover the entire globe and in our study serve to assess the FLH in the free atmosphere using air temperature from different geopotential heights. The levels around the FLH (500, 550, 600, and 650 hPa) were examined for a transition from a positive to a negative temperature (similar to *Bradley et al.* [2009]). Free-air FLHs were then linearly interpolated from the geopotential heights of the transition levels. The high spatial resolution of MERRA2 (0.5°) may for some cases be a disadvantage in assessing FLH over mountainous terrain. In comparison to ERA-Interim, values lying below the topography are masked out in MERRA2. Due to the higher resolution, there are more grid points with the FLH lying below the Earth's surface, which leads to difficulties in interpolating a FLH. We did not consider the topography and extrapolated to a FLH even if the resulting FLH lay below the surface, as a potential future temperature rise may lead to an FLH that lies above the surface.

3.2. Meteorological Station Data

Meteorological ground-based measurements are provided by the Servicio Nacional de Meteorología e Hidrología del Perú (SENAMHI) and the Universidad Nacional Santiago Antúnez de Mayolo (UNASAM). A list of the stations is given in Table S1 in the supporting information. The SENAMHI operated a relatively dense national network of meteorological stations since 1964. Air temperature is provided as daily T_{max} and T_{min}

Table 1. Data Types Used for Assessing FLH and SLH and Used Variables (P: Precipitation, T: Air Temperature, H: Geopotential Height, BB: Bright Band Height)

Data Type	Variable	Selected Time Period for Analysis	Spatial Resolution	Temporal Resolution	Used for
ERA-Interim reanalysis	*P*, *T*, *H*	1980–2015	0.75° (~82 km)	6 h	FLH
MERRA2 reanalysis	*T*, *H*	1980–2015	0.5° (~56 km)	3 h	FLH
Ground station measurement SENAMHI	*P*, *T*	1964–2015 (depending on station)	Point measurements	Daily	FLH
Ground station measurement UNASAM	*P*, *T*	2012–2015	Point measurements	1 h	FLH
Ground station measurement METAR	*T*	1996–2015	Point measurement	1 h	FLH
TRMM 2A23 Precipitation Radar	*BB*	1997–2015	Variable spatial resolution[a]	Variable temporal resolution[a]	SLH
MRR	Doppler velocities, reflectivity	Aug 2014 to Feb 2015	Point measurement	1 min	SLH

[a]See, *Schauwecker et al.* [2016].

(and additionally measured at 07:00, 13:00 and 19:00 local time), and precipitation is measured once a day, which makes it difficult to estimate the FLH only during precipitation events. The UNASAM runs a network of 16 meteorological stations located in the region of the CB (Ancash) since 2012. The hourly resolution allows distinguishing between the FLH for all hours and during precipitation events. Additionally, we used data from the METAR station located at the airport in Cusco (71.97°W/13.55°S). METAR records can be downloaded, e.g., from the National Oceanic and Atmospheric Administration [*National Oceanic and Atmospheric Administration*, 2016].

Station data are scarce at high elevations, but lower elevation stations can be used to assess the FLH and SLH using simple extrapolation techniques with either constant lapse rates (assuming, e.g., −0.0065°C/m; Figures 4 and 5) or by linearly extrapolating where several stations are recording (Figure 6). For the analyses in Figure 6, we considered stations located at elevations above 3500 (3000) m asl in the area of the CV (CB). We only considered station data from days (SENAMHI data) or hours (UNASAM data) where precipitation was registered, in order to assess the FLH for wet conditions. The FLH was then extrapolated on a daily (hourly) basis from these stations using linear regression, but only where data of at least four (three) stations were available for SENAMHI (UNASAM) data. Table S1 provides information on the utilized SENAMHI and UNSAM stations used.

3.3. TRMM Precipitation Radar Bright Band Data

In addition, we used Bright Band (BB) heights from the Tropical Rainfall Measuring Mission (TRMM) by the National Aeronautics and Space Administration (NASA) and the Japan Aerospace Exploration Agency (JAXA) to assess the snow/rain transition height. The BB is a zone of enhanced radar reflectivity, which is commonly observed in precipitation radar (PR) images during precipitation events. This zone of intensified echoes is caused by a horizontal melting layer in the atmosphere, at the height where ice or snow particles are transformed into liquid raindrops [e.g., *Battan*, 1973]. TRMM BB heights are given in the product 2A23 and are available for the 17 years of active TRMM measurements (1997–2015). The possibilities and limitations of using TRMM 2A23 BB heights for mountainous regions are described in, e.g., *Schauwecker et al.* [2016], who found for instance that the data availability is generally limited over high mountain regions. Over the CB and CV, the BB is too close to the surface, and thus disturbed by the ground echo [*Schauwecker et al.*, 2016]. However, over the Amazon lowlands, TRMM 2A23 BB heights have the potential to provide valuable information on the seasonal variability of the SLH.

3.4. Micro Rain Radar Data

From August 2014 to February 2015, a MRR was installed in the city of Cusco, (13.5278°S, 71.9508°W) at the SENAMHI office (at a distance of ~1 km from the Airport [see also *Perry et al.*, 2017]). We compute the altitude of the melting layer using the minute-resolution MRR data and an algorithm that includes several checks to filter unrealistic values. The first removes periods of positive velocity and reflectivity gradients (from lower altitudes to higher altitudes) due to the fact that melting layers will always involve negative gradients of these two values. Periods of virga are then discarded to prevent the algorithm from utilizing gradients at the bottom of the precipitation. Time periods when the most negative gradient in reflectivity is not within 300 m above the most negative gradient in velocity are then discarded. This is to ensure that unrealistically thick melting layers are not processed by the rest of the algorithm. Once the data are run through these filters, aspects of the melting layer are calculated. As a snowflake falls through the atmosphere from temperatures below freezing to above freezing, water droplets form on the outside of the flake. This increases the radar-detected reflectivity due to the higher dielectric constant of water than of ice. Once melting is complete, the denser raindrop will fall at a higher velocity than the previous snowflake. Using these principles, the algorithm identifies the bottom of the melting layer as the most negative gradient in velocity in the profile and the top of the melting layer as the most negative gradient in reflectivity. The melting layer height is then computed as the most negative gradient in velocity plus the average melting layer thickness for the respective hour of the storm. Finally, the results of the melting layer height algorithm are passed through two more checks. The first discards values above 6000 m, since the FLH rarely exceeds this altitude even in the tropics. The second discards any values outside of one standard deviation of the mean for the hour in which it lies. The values that are used in this study are the hourly median melting layer heights which are computed from the original minute-resolution values.

3.5. Global Climate Model Data

To assess the FLH by the end of this century over the mountainous regions of Peru, we analyzed GCM simulations. The resolution of most GCMs does not adequately resolve the complex topography of the Andes. We therefore analyzed FLH changes of the free troposphere (according to, e.g., *Bradley et al.* [2004] and *Bradley et al.* [2009]). The FLH change is taken from models which were part of the Coupled Model Intercomparison Project 5 (CMIP5) [*Taylor et al.*, 2011]. We compared the runs representing present-day climate (1976–2005; "historical" experiment) to the climate by the end of 21st century (2071–2100), taking the most optimistic (low emissions) and pessimistic (high emissions) Representative Concentration Pathways (RCP) 2.6 and 8.5, respectively [*Moss et al.*, 2010]. The RCP2.6 is called "peak-to-decay" scenario, in which radiative forcing reaches a maximum near the middle of the 21st century before decreasing to an eventual nominal level of 2.6 W m^{-2} relative to preindustrial conditions. Under RCP8.5, the radiative forcing is assumed to increase throughout the 21st century until reaching a level of 8.5 W m^{-2} at the end of the century relative to preindustrial conditions [*Taylor et al.*, 2011]. We use a 24-member ensemble of CMIP5 model simulations. A list of the models used is given in Text S1 in the supporting information. Similar to the analysis of reanalysis data, we estimated the FLH based on the temperature of different pressure levels (400, 500, 600, and 700 hPa). The increase of the FLH is then estimated as the difference between the historical runs (average over 1976–2005) and the end-of-century projections (2081–2100).

3.6. Glacier and Elevation Data

To assess whether regional differences in glacier extents are linked to the FLH, we computed glacier hypsographies in 100 m elevation bins, using glacier outlines from the Global Land and Ice Measurements from Space [*Global Land and Ice Measurements from Space and National Snow and Ice Data Center*, 2005] and the Unidad de Glaciología y Recursos Hídricos (UGRH) glacier database and Advanced Spaceborne Thermal Emission and Reflection Radiometer (ASTER) digital elevation models (DEM) [*NASA Jet Propulsion Laboratory*, 2009]. We do not consider any potential vertical error of the ASTER DEM in this study. Outlines are based on satellite images from 2003 and 2005 for the CB [*Racoviteanu et al.*, 2008] and from 2000 (Global Land and Ice Measurements from Space (GLIMS) inventory) and 2009 (UGRH inventory) for the CV. Based on the hypsographies we then assessed the median elevation of glaciers as well as the fraction of glacier area below the present-day wet season (December-January-February (DJF)) FLH from reanalysis data. The present-day wet season FLH is then illustrated in a map, as well as the FLH by the end of this century under RCP2.6 and RCP8.5.

4. Results

4.1. Present-Day Freezing and Snowfall Level Height From Multiple Data Types

First, we present an overview of the FLHs and the regional and seasonal variability derived from reanalysis data. Seasonal present-day (1980–2015) FLHs over Peru based on ERA-Interim and MERRA2 reanalysis data are shown in Figure 3. The MERRA2 FLH generally lies higher than the ERA-Interim FLH over the study areas and the Andes (see also Figure S1 in the supporting information). Both data sets have similar regional pattern: the FLH is higher over Southern Peru and Bolivia, as well as at the Peruvian coast, compared to the lower FLH over Northern Peru and the Amazon basin. According to the overall pattern, the FLH is higher over the CV than the CB. The results further show that the FLH is lowest during the dry season (June-July-August (JJA)) and highest during the wet season (DJF).

Figure 4 shows the reflectivity of three rainfall events from different months during the transition and wet season (7/8 October 2014, 9 December 2014, and 18/19 January 2015). We selected these events, because the duration was at least 3 h and the transition from solid to liquid precipitation was clearly visible. Figure 4 further shows the estimated SLH based on the MRR data, as well as the ERA-Interim and MERRA2 FLH and the extrapolated FLH based on data from one meteorological station, using a constant lapse rate (−0.0065°C/m). The three figures show that at the beginning of the precipitation events, the extrapolated FLH clearly lies above the SLH derived from the MRR data. After approximately the first hour of strong precipitation, the extrapolated FLH drops and approaches the SLH derived from MRR data. These results illustrate that the accuracy of the snow/rain transition estimation based on air temperature extrapolation strongly depends on the time of the measurements and likely improves after the first few hours of the precipitation event. The reanalysis FLHs lie in all cases above the SLH, whereas the MERRA2 FLH is found at higher altitudes than the ERA-Interim FLH, according to Figure 3.

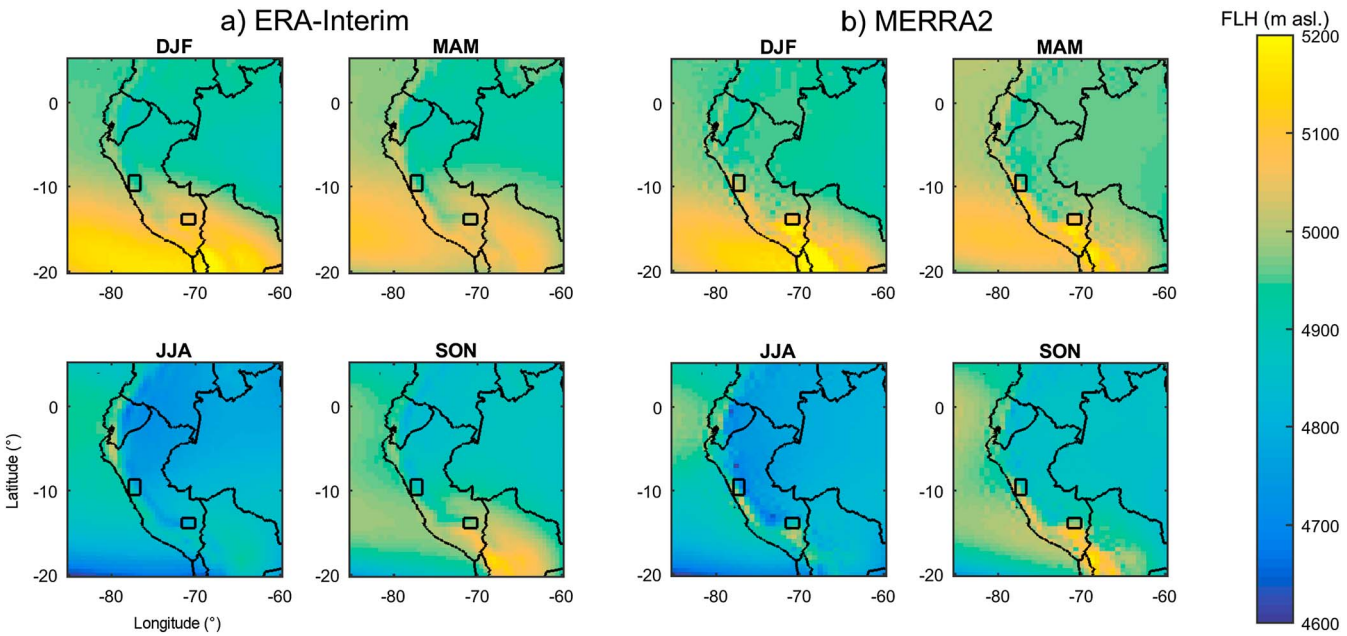

Figure 3. Mean present-day (1980–2015) seasonal (a) ERA-Interim and (b) MERRA2 FLH (m asl). The areas of the CB and CV are marked with black boxes.

We then compared the MRR SLH data from all recorded precipitation events to FLH obtained from ERA-Interim and MERRA2 reanalysis data (Figure 5a) as well to the extrapolated FLH (Figure 5b). The MRR SLH ranges in 95% of the cases between 4430 and 5160 asl ($\mu \pm 2\delta$; Figure 5a). As expected, the correlation between the SLH and reanalysis FLH is rather low (R^2 = 0.26 and R^2 = 0.10, for ERA-Interim and MERRA2, respectively). The radar-derived SLH lies on average 220 m below the ERA-Interim FLH and 240 m below the MERRA2 FLH. The spread is considerable (δ = 172 and 202 m, for ERA-Interim and MERRA2, respectively). Only in few cases was the SLH higher than the FLH, indicating that liquid precipitation rarely occurs above the reanalysis FLH. In Figure 5b we see that the extrapolated FLH represents relatively well the SLH for low air temperatures at the ground (below approximately 15°C). In contrast, the extrapolated FLH strongly overestimates the SLH for high temperatures above approximately 15°C. Figure 5b indicates that high temperatures are in most cases occurring within the first 5 h of the precipitation events, as shown in Figure 4.

Figure 6 presents FLHs and SLHs for the CB and CV based on multiple data types. All data sets show a clear seasonal variability with lower FLHs and SLHs during the dry season (JJA). The different data types indicate that the seasonal variability is stronger for the CV than the CB. The stronger seasonality is especially visible for the extrapolated FLH from station measurements (Figure 6h). The extrapolated FLH in the CB (Figure 6c) shows a much lower annual variability compared to reanalysis data (Figures 6a and 6b). In contrast, the FLH based on UNASAM station data (Figure 6d) have a much larger variability and spread compared to the SENAMHI data (Figure 6c), probably due to the hourly resolution of the UNASAM data (compared to the daily resolution of SENAMHI data). The difference between the extrapolated FLH from ground stations (Figures 6c and 6h) and the free atmosphere FLH from reanalysis data (Figures 6a, 6b, 6f, and 6g) is about 310 m for the CB and 220 m for the CV. For the dry season (JJA) in the CV, the extrapolated FLH (Figure 6h) lies up to 390 m below the reanalysis free atmosphere FLH (Figures 6f and 6g). There seems to be a regional difference in FLH between the CV and CB. The FLH from reanalysis data lies on average about 110 m higher for the CV (Figures 6f and 6g) than for the CB (Figures 6a and 6b), with a larger difference of 150 m during the wet season. During the dry season (JJA) this difference is much smaller or even negligible (approximately 50 m). During the wet season, the mean FLH from reanalysis is around 4950 (5090) m asl for the CB (CV), in line with the overall pattern identified in Figure 4.

ERA-Interim reanalysis data (Figures 6b and 6g) show that FLHs during precipitation events agree well with the FLH for all days during the wet season and the transition periods. Only during the dry season (JJA), the event-based FLH lies below the mean FLH of all days, the difference being larger for the CV. Also, the extrapolated FLH of all hours and wet hours agrees well (Figure 6d). As expected, due to few precipitation events

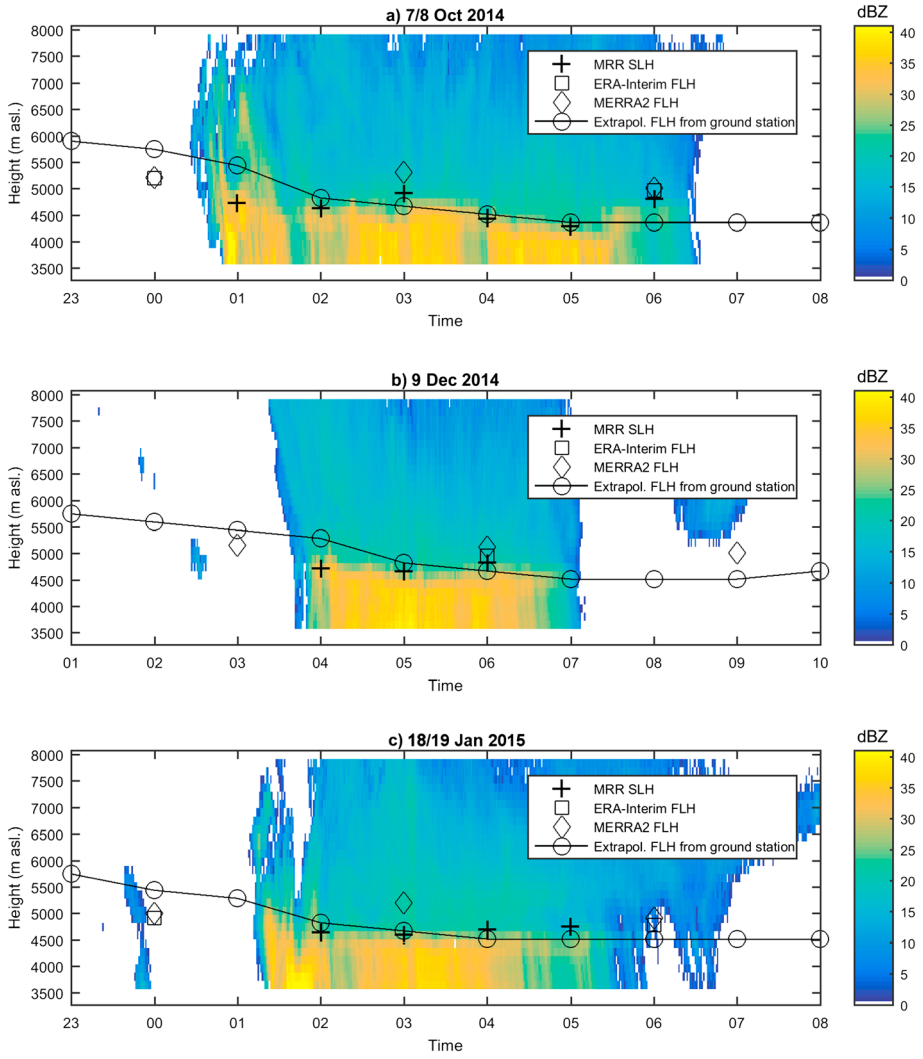

Figure 4. MRR reflectivity of three precipitation events over the city of Cusco registered on 7/8 October 2014, 9 December 2014, and 18/19 January 2015. Indicated are simulated SLHs from MRR and FLHs from ERA-Interim and MERRA2 reanalysis, as well as extrapolated FLH from the meteorological ground station.

during the dry season and the relatively short measuring period, it was not possible to assess accurately the dry season FLH during precipitation events.

TRMM PR BB data are only available for the Amazon basin and the foothills adjacent to the mountain regions, which makes a direct comparison to the MRR data difficult. Compared to the reanalysis FLH over the study areas (Figures 6a, 6b, 6f, and 6g), the SLHs derived from BB heights from TRMM over the Amazon basin lie approximately 500 m (CB) to 600 m (CV) lower (Figures 6e and 6j). This difference is comparable to results from other studies from the Himalaya [e.g., *Thurai et al.*, 2003; *Awaka et al.*, 2009; *Schauwecker et al.*, 2016].

Hence, these multiple data types show a clear but—compared to midlatitudes—low seasonality in the FLH and indicate a regional difference between the CB and the CV. However, the difference of the FLH among the different data products is considerable and points to the need of multiple data analyses to get a reliable FLH assessment.

4.2. Future Freezing Height From CMIP5 Model Results

We used CMIP5 model results to assess the expected FLH changes by the end of this century (2071–2100). For both regions, the CMIP5 models project a strong FLH increase (Figure 7). The model results show a remarkable difference between the two scenarios. While the multimodel median FLH increase is on average 230 m

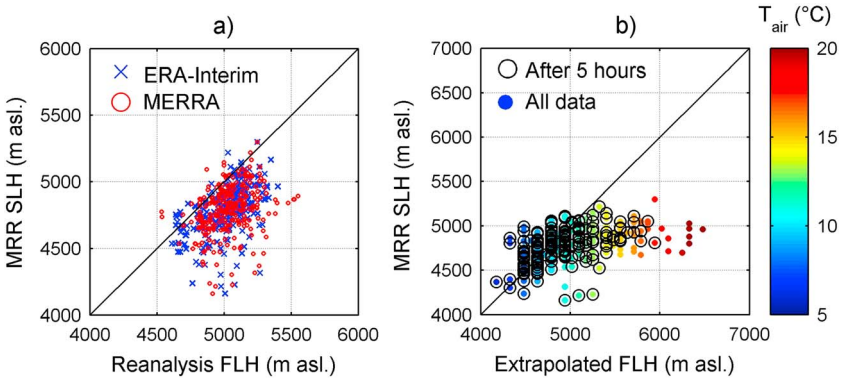

Figure 5. (a) MRR SLH estimations versus ERA-Interim and MERRA2 FLH; (b) MRR SLH estimation versus extrapolated FLH based on air temperature measured at the METAR station in Cusco. The color scale in Figure 5b expresses air temperature measured at the METAR meteorological station.

for RCP2.6, it is 850 m for the most pessimistic scenario RCP8.5. The spread between the single model results is considerable, ranging within approximately 40 to 420 m for RCP2.6 ($\mu \pm 2\delta$, 2δ = 190 m) and 460 to 1240 m ($\mu \pm 2\delta$, 2δ = 390 m) for RCP8.5. The increase is strongest during the dry season (JJA) for most models under the emission scenario RCP8.5. The stronger climb in the dry season is not visible under RCP2.6.

Slight regional differences for the projected FLH increases are visible in Figure 8. The multimodel results for RCP8.5 indicate that the FLH is predicted to increase by ~900 m over Ecuador, especially during the dry season (JJA). Over the Altiplano in Southern Peru, the increase is slightly smaller but still over 700 m.

Glacier hypsographies provide valuable information on glacier elevation distribution and allow relating the glacier covered area to the observed regional differences in the FLH. Both regions show a similar pattern of altitudinal distribution, but the elevation of glaciers in the CB is shifted down to lower elevations compared

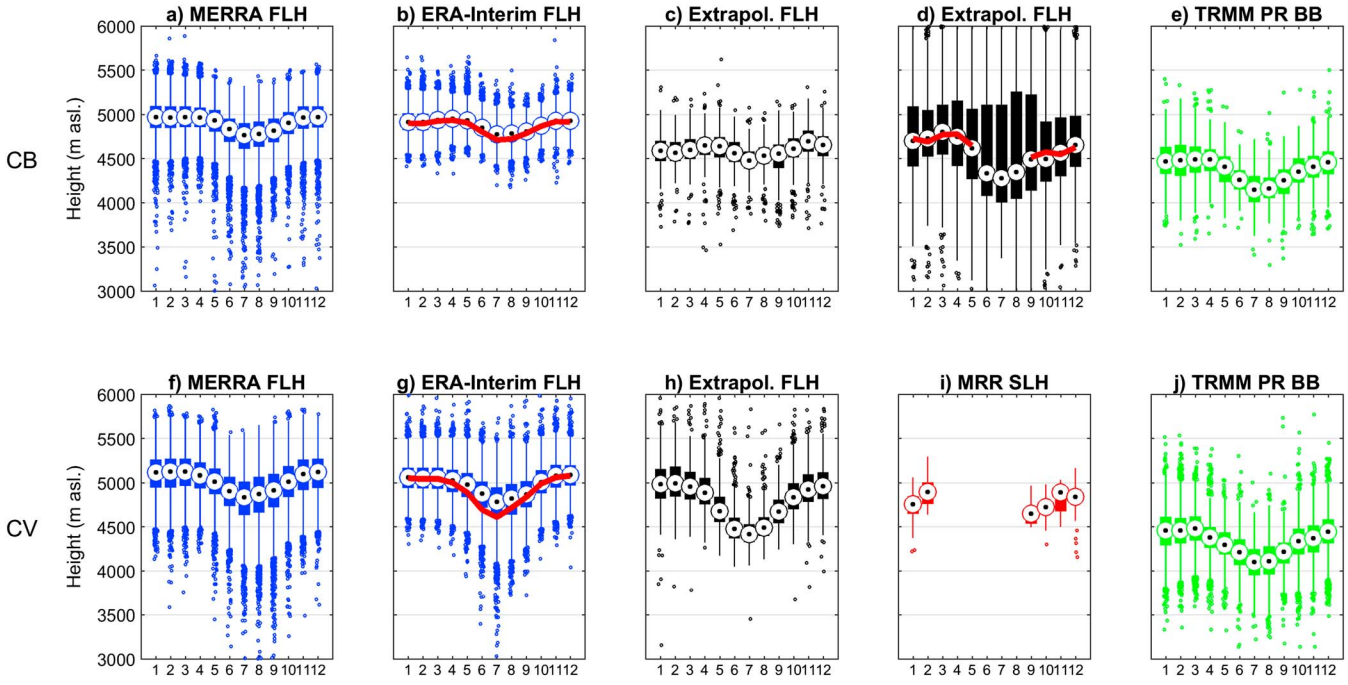

Figure 6. Monthly FLHs and SLHs (January to December) for the (a–e) CB and (f–j) CV from different data sources: MERRA2 FLH (1980–2015) (Figures 6b and 6f), ERA-Interim FLH (1980–2015) (Figures 6b and 6g), and FLH extrapolated from SENAMHI stations (1994–2015, CV and 1998–2015, CB) (Figures 6b and 6h) as well as from UNASAM stations (Figure 6b), SLH estimated with MRR data (September 2014 to February 2015) (Figure 6b), TRMM BB heights (1997–2015) (Figures 6b and 6j). The red lines in Figures 6b, 6d, and 6g represent the median of the FLH during precipitation events. The circles represent the median, the boxes represent the 25th and 75th percentiles, the whiskers represent 1.5 standard deviations, and the outliers are plotted with points.

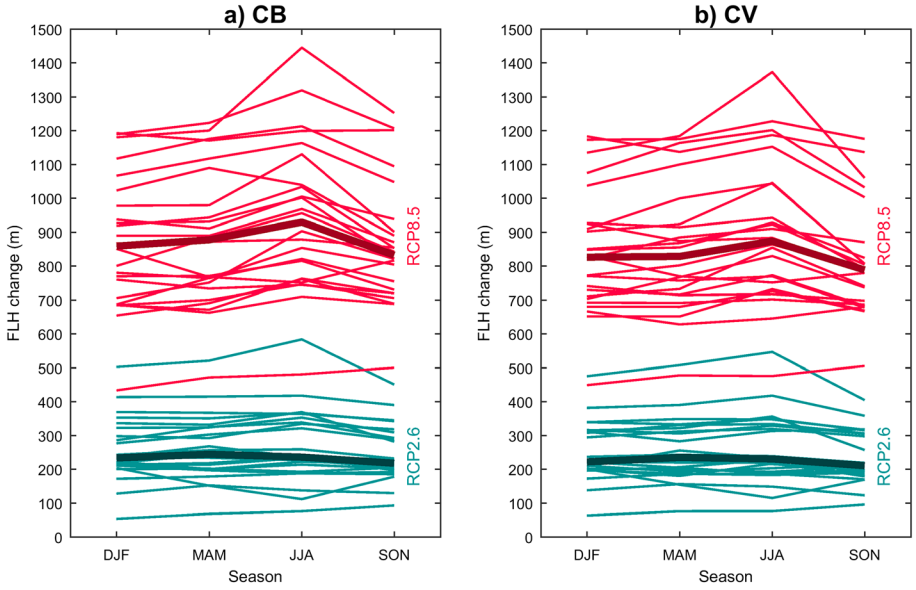

Figure 7. Projected future FLH change for the grid cell closest to the (a) CB and (b) CV for RCP2.6 (green) and RCP8.5 (red). Each line represents the results of one model (see list in the supporting information), and the thick dark lines represent the median of all model results.

to glaciers in the CV (Figure 9). The median elevation of glaciers in the CB is 126 m lower compared to the CV, respectively. In Figure 9, we also plotted the mean wet season (DJF) FLH and SLH from ERA-Interim and MERRA2 data. From the results in Figure 5, we suggest that the SLH lies on average about 220 m and 240 m below the ERA-Interim and MERRA2 FLH, respectively, so the mean wet season SLH lies at about 4700 and 4900 m asl, for the CB and CV, respectively. For both regions, the SLH is the approximate altitude below which no glaciers exist. According to the glacier inventory data used only 4% (1%) of the total glacier

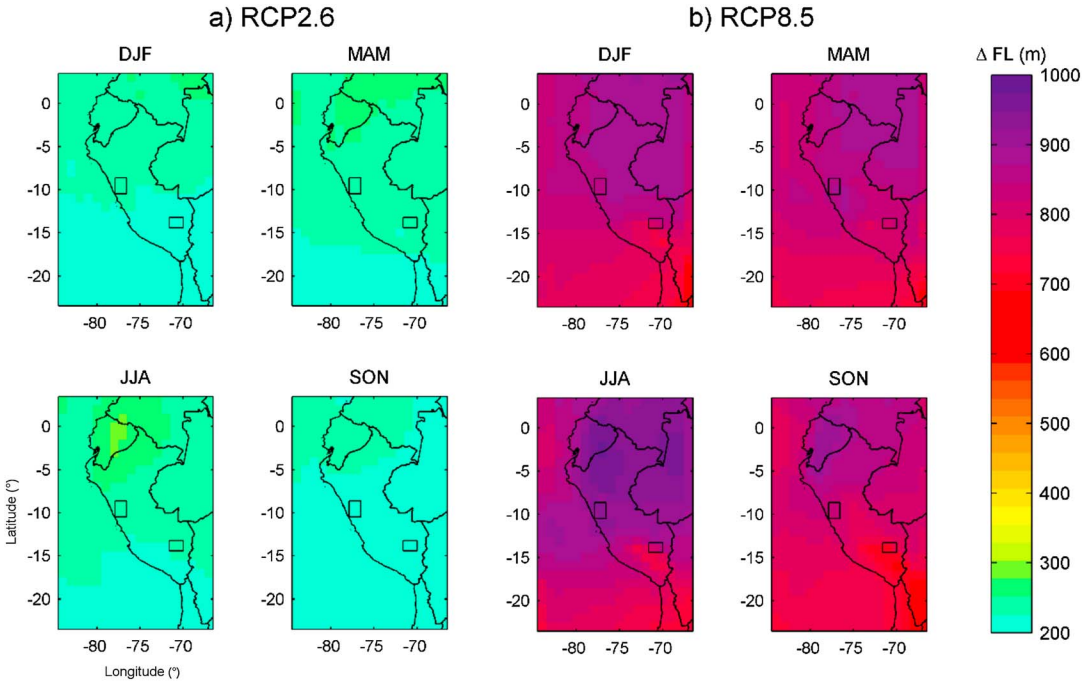

Figure 8. Multimodel median of projected future FLH level change for the region of the Peruvian Andes during DJF, March-April-May, JJA, and September-October-November for (a) RCP2.6 and (b) RCP8.5 between 1976–2005 and 2081–2100. The areas of the CB and CV are marked with black boxes.

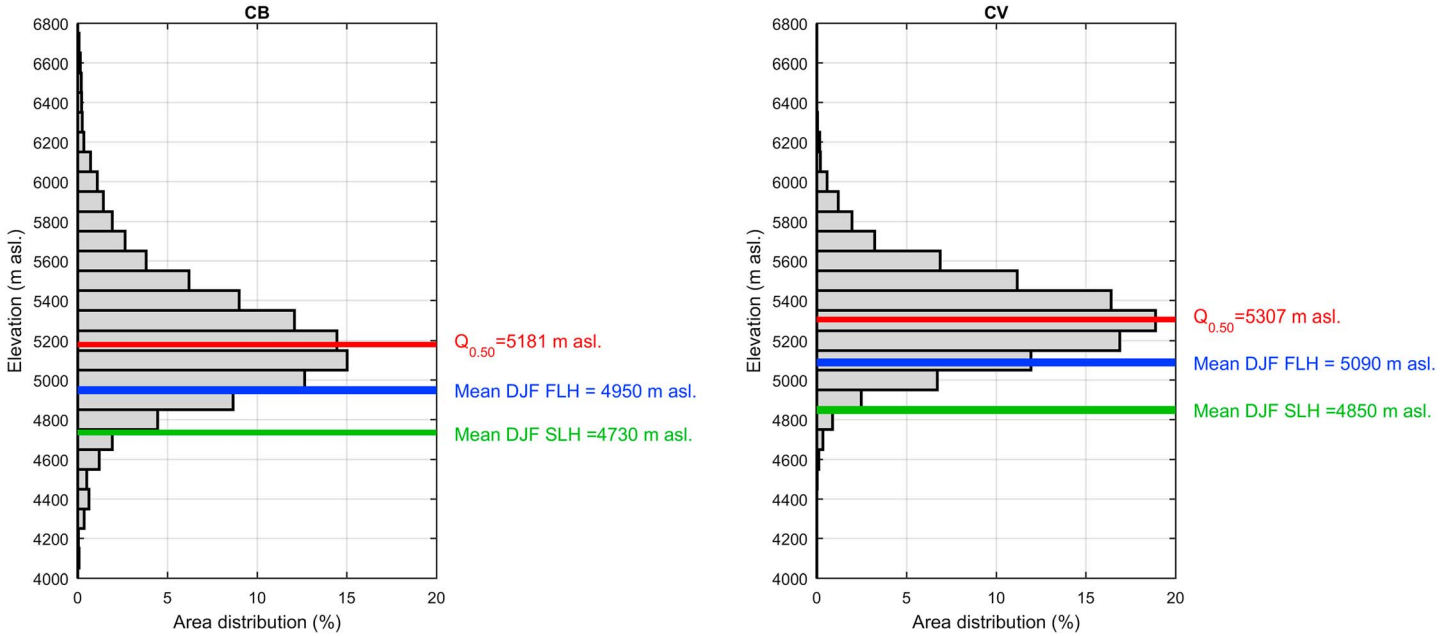

Figure 9. Glacier hypsographies for (a) CB and (b) CV. The red lines show the median elevation of the glacier-covered area; the blue lines show the mean estimated present-day wet season (DJF) FLH based on ERA-Interim and MERRA2 reanalysis data; the green lines show the mean estimated present-day wet season (DJF) SLH.

area of CB (CV) lies below this elevation. Both reanalyses clearly show that the wet season FLH lies about 150 m higher in the CV compared to the CB. It can be seen from the hypsographies that the wet season FLH approximately corresponds to the 17% (15%) quantile of the elevation distribution for the CB (CV), meaning that only ~17% (15%) of the total glacier area is below the wet season FLH, indicating a relation between the wet season FLH and glacier extents.

Figures 10 and 11 show the present-day glacier extent as well as the present-day and end-of-century wet season FLH under RCP8.5 and RCP2.6. Mainly tongues of relatively large glaciers, some of them debris-covered, exist below the altitude of the present-day wet season FLH, especially for the CB. On the southern side of CV, around the Sibinacocha lake, many glacier tongues are ending at altitudes higher than the present-day FLH. The map also shows that in some areas around Sibinacocha lake there are no glaciers at all above the FLH, probably due to limited maximum elevation (~5300 m asl) in these areas implying insufficient accumulation areas for the existence of glaciers. The green areas show the area above the projected wet season FLH under the RCP2.6 scenario. The area above the projected FLH under RCP2.6 is about 40% of the area above the present-day wet season FLH (Table 2). In contrast, the area above the RCP8.5 FLH is very small and consists only of the highest peaks in the region (e.g., Huascarán in the CB and Ausangate in the CV; Table 2).

5. Discussion

In the following section, we discuss the spatial and seasonal variabilities of the FLH derived from different data types (reanalysis data, extrapolation of meteorological station data, and TRMM PR BB estimations). Further on, the change in FLH by the end of this century and possible impacts on glacier extents are discussed.

5.1. Present-Day Freezing and Snowfall Level Height

Reanalysis data are easily applicable tools to assess regional and seasonal variabilities in the FLH. Despite local biases between ERA-Interim and MERRA2 (Figure S1), the overall pattern of both reanalysis products consistently shows highest FLHs occurring in the wet season (DJF) and lowest FLHs during the dry season (JJA). This follows from the nature of the annual air temperature cycle with cooler mean air temperature during the dry period (see for instance *Schauwecker et al.* [2014]). We assume that the higher FLH over Southern Peru may be a result of the Bolivian high pressure system, present in the upper troposphere during austral summer (DJF). The higher FLH over the coast and Southern Peru is in agreement with the FLH observed by *Bradley et al.* [2009] based on NCEP/NCAR data. *Diaz et al.* [2014] found a mean FLH of ~4500 m asl over the tropics,

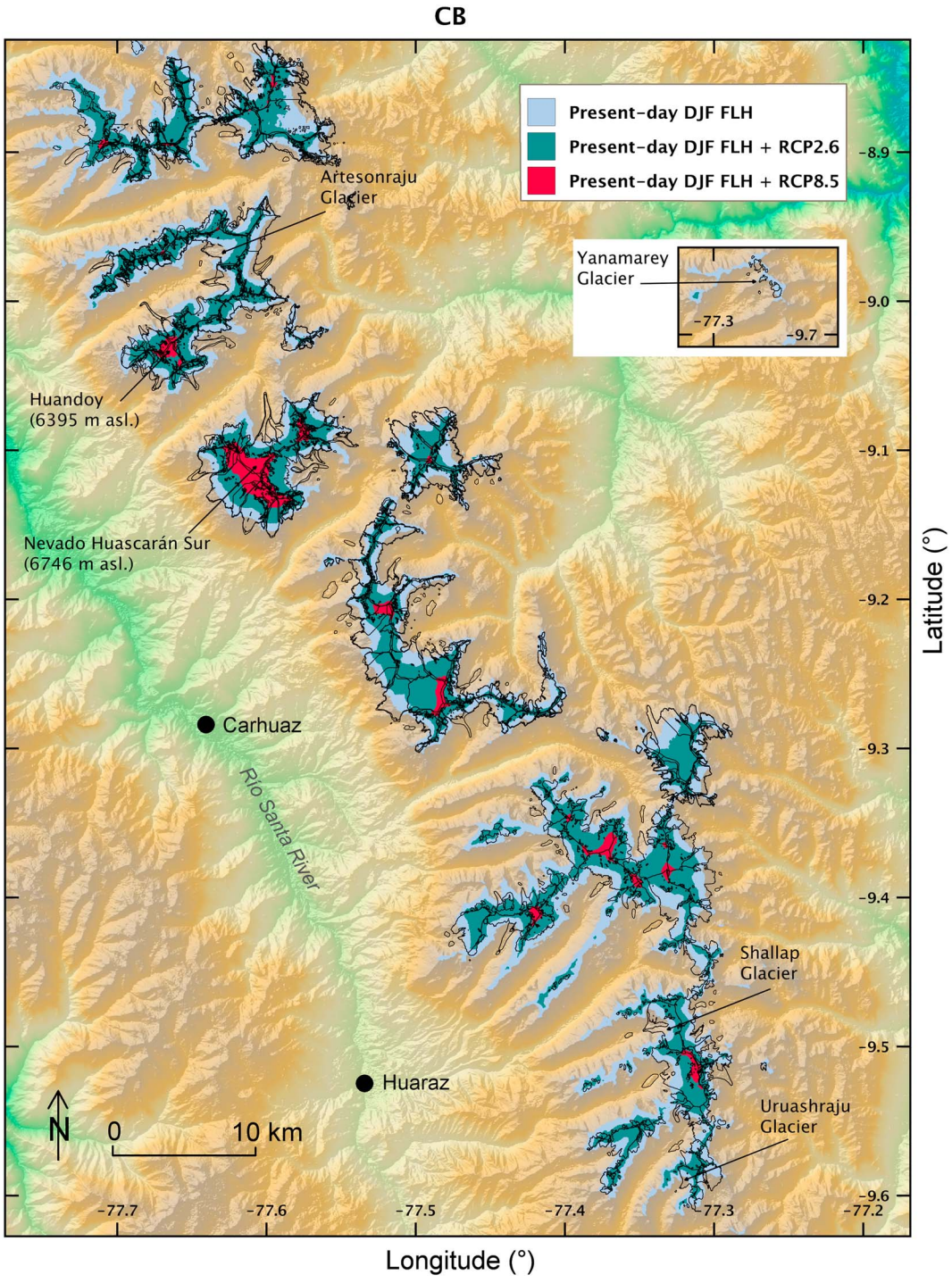

Figure 10. Glaciers in the CB with the area above the present-day FLH (light blue) and the area above the mean end-of-century FLH from the multimodel median model runs under emission scenarios RCP2.6 (green) and RCP8.5 (red). The black lines represent modern glacier extents.

based on NCEP/NCAR reanalysis data from 1973 to 2002. Therefore, our results indicate that the mean FLH of about 4900 and 5010 m asl in the CB and CV, respectively, may lie above the mean tropical FLH. These results are consistent with *Rabatel et al.* [2013], who found annual FLHs in the CB in the range of 4830 to 5000 m asl, with individual values of up to 5100 m asl. ERA-Interim data indicate that the FLH is on average lower during precipitation events. This difference is only visible during the dry season. The FLH can drop to considerably

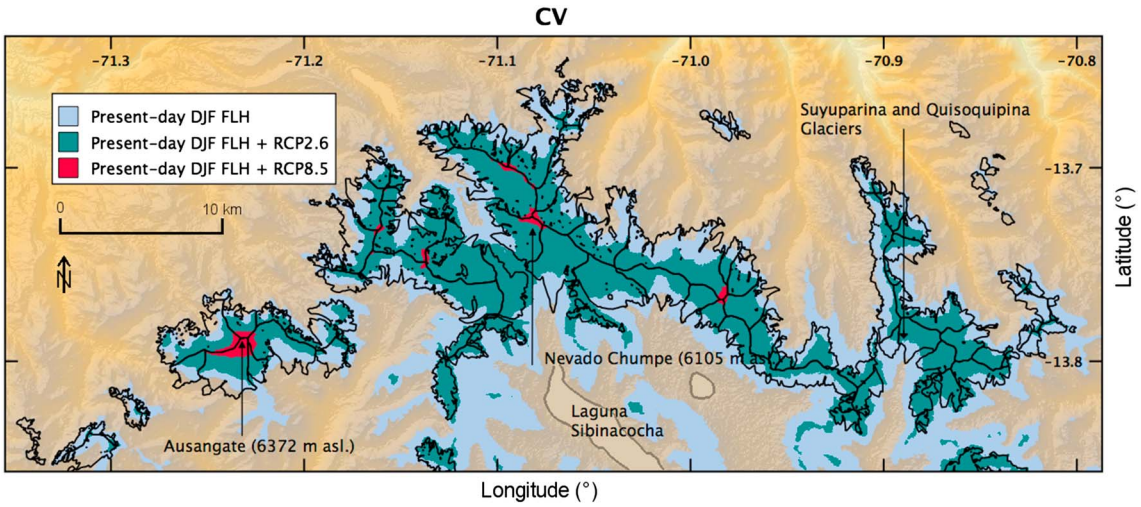

Figure 11. Glaciers in the CV (black lines) with the area above the present-day FLH (light blue) and the area above the mean end-of-century FLH from the multimodel median model runs under emission scenarios RCP2.6 (green) and RCP8.5 (red). The black lines represent modern glacier extents.

low altitudes (<3500 m asl) during the infrequent dry season precipitation events. Additionally, we found a correlation between reanalysis FLH and radar-derived SLH. The SLH lies generally below the reanalysis FLH. Other studies have also shown that the SLH (derived by TRMM PR BB) lies some hundreds of meters below the reanalysis FLH [*Harris et al.*, 2000; *Thurai et al.*, 2003; *Awaka et al.*, 2009] or the radiosonde FLH [*Schauwecker et al.*, 2016]. We conclude that reanalysis data are useful tools to assess the SLH, assuming that in our study region the SLH lies on average about 220 m and 240 m below the ERA-Interim and MERRA2 FLH, respectively. At single glacier, various factors (e.g., katabatic winds, aspect, and insolation) may influence local lapse rates. The here presented regional estimation of FLH and SLH is therefore associated with considerable uncertainties for a single precipitation event or at a certain point in time.

We found a relatively good agreement between radar-derived SLH and FLH estimation using extrapolation techniques (based on air temperature from a single meteorological station and a constant lapse rate of −0.0065°C/m). However, the bias increases significantly with higher air temperatures at the station, and the SLH is often strongly overestimated using extrapolation techniques above a near-surface temperature of around 15°C. Our results further indicate that the extrapolation is not very accurate if the air temperature is measured at the beginning of the rainfall event when the near-surface air temperatures are still high, similar to the conditions in the Indian Himalayas [*Schauwecker et al.*, 2016]. The extrapolation based on several meteorological stations using linear regression gets difficult for regions with few stations available. Additionally, the temporal resolution of conventional meteorological stations hampers the assessment of the FLH and SLH during precipitation events, since precipitation events in this region can be often rather short (minutes to hours). Another uncertainty exists in the estimation of the air temperature at the snow/rain transition. A threshold of 1.5°C is often used [e.g., *Klok and Oerlemans*, 2002]; however, we found that a threshold of 0°C might be more adequate for the Central Andes if compared to the radar-derived SLH of the free atmosphere.

Table 2. Current Glacier Extents and Areas Above the Current Wet Season FLH and the Mean End-of-Century FLH Under RCP2.6 and RCP8.5 (CB: 13.4°S to 13.86°S and 70.79°W to 71.37°W, UGRH Inventory; CV: 8.74°S to 9.88°S and 77.14°W to 77.86°W, GLIMS Inventory)

	Cordillera Blanca		Cordillera Vilcanota	
	(km^2)	(%)[a]	(km^2)	(%)[a]
Current glacier extent	457	–	223	–
Area above the current wet season FLH	614	100	374	100
Area above mean end-of-century FLH under RCP2.6	260	42	155	41
Area above mean end-of-century FLH under RCP8.5	7	1	13	3

[a]Respective to the current area above the wet season FLH.

We found that the TRMM PR BB lies on average about 500 to 600 m below the FLH from reanalysis data which agrees with other studies [e.g., *Harris et al.*, 2000; *Schauwecker et al.*, 2016]. We also found a limited TRMM PR BB data availability over the high mountain regions in Peru, as already described in *Schauwecker et al.* [2016] for the Indian Himalayas. However, the data provided over the foothills of the Andes and the Amazon basin serve as a complementary information source to assess for example the annual variability of the SLH. The variability of the BB height agrees well with the annual variability of the FLH derived by reanalysis data in these regions.

Our findings agree with more anecdotal evidence, such as observations of the snow/rain transition at the elevation of glaciers in the CB and the CV. For instance, it has been observed that during the wet season, there was almost exclusively rain on the tongue of Yanamarey glacier located at around 4680 m asl (according to the GLIMS inventory [*Racoviteanu et al.*, 2008]). In contrast, during the dry period, solid precipitation frequently occurred below the glacier terminus [*Kaser and Osmaston*, 2002]. Also, the tongue of Suyuparina glacier (CV) at approximately 5100 m asl was covered by a relatively thick layer of compact snow or firn in July 2011 and August 2014 and 2015 (observations made by the authors), indicating low snow/rain transition levels during the dry season. Moreover, present weather sensor measurements indicate that in the CV at 5050 m asl, precipitation is predominantly solid (94% of all precipitation hours during July 2012 to June 2014 [*Poremba et al.*, 2015]).

5.2. Future Freezing Height

We found that under RCP2.6, the mean future increase of the FLH is approximately 24 m per decade (±20 m, 2δ), agreeing with the observed 30 m per decade between 1955 and 2011 by, e.g., *Rabatel et al.* [2013], but being higher than the observed ~14 m per decade for the entire tropics (1958–2000 [*Diaz et al.*, 2003]). This means that even under the most optimistic scenario, the FLH in the Peruvian Andes will continue increasing at a similar rate as in the last about five decades. With RCP8.5, the future increase is extremely high with approximately 89 m per decade (±41 m, 2δ), meaning that the increase rate would be three times higher than the observed increase since the 1950s.

The results from Figure 8 show that the expected rise in the FLH over the Peruvian Cordilleras is rather homogeneous in space, probably a result of the spatial model resolution. However, the warming at the elevation of glaciers may be stronger than at low altitudes [e.g., *Bradley et al.*, 2004], which we could not show based on the FLH of the free atmosphere. *Diaz et al.* [2014] found similar increases in the FLH by the end of this century for the latitude of 10–15°S with about 900 m for DJF and 1000 m for JJA. *Bradley et al.* [2006] and *Vuille et al.* [2008] found a warming of 4.5–5°C by the end of the century, considering a similar radiative forcing relative to the preindustrial as RCP8.5 (using the SRES A2 scenario [*Intergovernmental Panel on Climate Change (IPCC)*, 2013]). Assuming a lapse rate of 0.0065°C/m, this temperature increase would thus correspond to a rise in the FLH of about 690 to 770 m, slightly below the increase presented here for the most pessimistic RCP8.5 scenario. Also for other regions in the world, the rise in SLH will be remarkable under RCP8.5. For example, *Viste and Sorteberg* [2015] found that the SLH will move upward by 700–900 m in the Indus, Ganges, and Brahmaputra basins, similar to our findings.

The FLH is closely related to El Niño–Southern Oscillation (ENSO) in the tropics [*Bradley et al.*, 2009], including the Andes of Ecuador [e.g., *Francou et al.*, 2004]. This relation might also be valid for the Peruvian Andes [e.g., *Vuille et al.*, 2008, *Maussion et al.*, 2015]. CMIP5 GCMs exhibit a range of behaviors for ENSO variability in the future, some showing an increase in ENSO variability, others a decrease, and some no change [*Guilyardi et al.*, 2012]. If ENSO events become more frequent in the future, the FLH rise could be even stronger than projected by the mean of all CMIP5 models. Moreover, as suggested by *Tan et al.* [2016], CMIP5 models may strongly underestimate mixed-phase cloud effects (Wegener-Bergeron-Findeisen process) under climate change. Also, this may lead to an even higher FLH than projected by RCP2.6 and RCP8.5. Increases in the FLH as a result of rising temperatures has led and will lead to a decline of the surface area above this critical level of mountainous regions around the world [*Diaz et al.*, 2003], having important impacts on, e.g., glacier recession as discussed in the following section.

5.3. Impact of Rising Freezing and Snowfall Level Height on Glaciers

We found that during the wet season (DJF), where most of the annual precipitation falls [e.g., *Kaser et al.*, 1990], the mean FLH from reanalysis data lies at approximately 4950 m asl (5090 m asl) for the CB (CV), see

also Figure 9. SLH analysis indicates that during most of the year snow is falling down to 40–420 m below this level (see Figure 5a). But snow below the FLH is melting or sublimating within few hours due to the positive temperatures and solar radiation [*Poremba et al.*, 2015]. Annual accumulation therefore likely only exists predominantly above the FLH. The FLH not only determines accumulation but it also largely influences net shortwave radiation via albedo effects. Where snow does not accumulate during the wet season, the glacier surface is mostly snow free and has thus a relatively low albedo. A large fraction of the incoming shortwave radiation is absorbed and not reflected, leading to large amounts of energy available for ablation. As a consequence, tropical glaciers are characterized by steep mass balance gradients below the FLH and high accumulation area ratios (compare to, e.g., *Kaser* [2001]). The high glacier ablation below the FLH thus exerts an important control on the glacier terminus. This explains why only approximately 15% of the current total glacier area is below the present-day wet season FLH for both regions (Figure 9). Dynamic ice flow effects become more important with larger glaciers with more extensive accumulation areas which thus can form glacier tongues reaching down to lower elevations as enough ice is flowing down to substitute the ice loss.

The FLH has been suggested as an approximation of the equilibrium line altitude (ELA) of glaciers, with the ELA dividing the area of mass loss and gain on a glacier averaged over 1 year [*Condom et al.*, 2007; *Rabatel et al.*, 2012; *Sagredo et al.*, 2014]. Here we analyzed the wet season FLH in relation with the glacier extents in reference to their lowermost elevations. Although at a local, single glacier scale there are considerable variations in this relation we found that a higher coherence of this relation at a regional scale. Furthermore, in consideration of the physical mass gain and loss processes effective at tropical glaciers it is reasonable to assume that an increase of the FLH has a proportional effect on glacier areas. Thus, if we assume that the percentage of glacier area below the wet season FLH remains similar in the future, glaciers will lose more than half of their area under the most optimistic scenario RCP2.6 (see Figures 10 and 11 and Table 2). If the temperature increases as much as under RCP8.5, there will be only some small glaciers left on the top of the highest mountain peaks in both regions. Especially small, low-elevation glaciers will first disappear, as well as glaciers with low-lying accumulation areas. These findings are in the same range as results from *Juen et al.* [2007], who simulated changes in glacier extent using a model based on a vertical mass balance profile model [*Kaser*, 2001]. They showed that under the B1 (low) emission scenario [*IPCC*, 2000], glaciers in the Llanganuco catchment (86.4 km^2) in the CB would lose about 49% of their area in 2080 compared to 1990. The area loss would increase to 75% under the (pessimistic) A2 scenario.

To fully explain future glacier extents, an energy balance model including glacier dynamics would be needed, requiring different parameters which are typically not available at high altitudes and/or related to large uncertainties. Single glaciers may respond differently to changes in the FLH, depending on their aspect, slope, elevation distribution, area, topographical location, etc. These glacier parameters are probably somewhat different for the CB and CV resulting in a regional difference in glacier retreat. Our projection for the future glacier extents therefore do not apply at the local glacier scale but rather represents an overall estimate for the glacier-covered area at a regional scale (for the CB and CV). Moreover, there might also be substantial changes in other meteorological variables like humidity, cloud cover, precipitation, and downwelling longwave radiation. However, all of these variables and their future changes are associated with uncertainties and a more detailed model will not necessarily offer more reliable results. For instance, due to the small-scaled topographic features of the Andes, the ability of GCMs to simulate precipitation is limited [e.g., *Minveille and Garreaud*, 2011]. *Neukom et al.* [2015] suggest that simulations using a relation between precipitation and the midtropospheric and upper tropospheric flow result in more reliable projections and that precipitation may decrease substantially by the end of this century. With decreasing precipitation, glacier retreat would be even stronger than discussed assuming only an increase in the FLH. Moreover, glaciers are already today out of balance with the current climate conditions [e.g., *Schauwecker et al.*, 2014], which was not considered in our experiment. *Rabatel et al.* [2013] stated that since a marked increase in FLH in the late 1970s, the ablation zones of glaciers in the CB are mostly located within the altitudinal range of the annual mean FLH. Even if warming halted for some decades, glaciers would continue shrinking for years or decades, depending on their response time. For example, larger glaciers like Artesonraju have response times of 10–40 years [e.g., *Schauwecker et al.*, 2014], while small and thin glaciers adapt much faster to the climatic conditions. Furthermore, once the FLH rises above the highest glacier extent, the lack of an accumulation area would lead to an even stronger melt down of the remaining

ice. Other feedback between the glacier and their environment could also lead to much more extreme glacier shrinkage than assumed here. Despite a number of uncertainties described above, we conclude that our estimate is a robust and even rather optimistic scenario.

Our experiment may only be valid for glaciers that are sensitive to air temperature, which is not the case for all tropical glaciers. Where air temperature is cold enough during the year for solid precipitation across the glacier, mass balance seems most sensitive to precipitation and moisture (e.g., in Bolivia [see *Kaser*, 2001]; *Favier et al.*, 2004a]). The dependence and sensitivity of glaciers to changes in the FLH are thus likely highest where tongues are already today close to 0°C around the year, namely, glaciers in Ecuador or Peru.

6. Concluding Remarks

In this study, we assessed the present-day FLH over the Peruvian Andes as well as the seasonal and regional variability, using multiple data sources. The SLH was estimated from MRR data in Cusco and related to FLH from reanalysis and extrapolated meteorological station data. We used CMIP5 scenario runs to estimate the change in FLH by the end of the 21st century compared to present-day and discussed possible impacts on glacier extents in the CB and CV—the two largest glacierized mountain ranges in Peru. The results enabled us to highlight the following conclusions:

1. Reanalysis data are suitable and easily applicable tools to assess the regional and seasonal variabilities of the FLH, and there is a reasonable correlation between reanalysis data and radar-derived snow/rain transition. However, for estimating SLH of a single precipitation event, reanalysis FLH data have to be used with caution mainly due to the coarse spatial resolution. The SLH derived from MRR estimates lies about 40–420 m below the reanalysis FLH (on average 220 m below ERA-Interim and 240 m below MERRA2). SLH estimates based on extrapolation techniques have to be applied with caution when relatively high air temperatures are measured at the beginning of the precipitation event. The air temperature threshold for the snow/rain transition has to be defined carefully, depending also on temperature measurement techniques. In our analysis, a lapse rate of −0.0065°C/m and a threshold of 0°C seems to be appropriate to estimate the free air snow/rain transition based on a single meteorological station. However, for the phase of near-surface precipitation a typical threshold of about 1.5°C might be more suitable. The methodology to assess the FLH and SLH using multiple data types has a potential to be enhanced, and the temporal and spatial resolutions of the FLH could be improved by using ground-based meteorological (e.g., UNASAM station data) or additional reanalysis data.
2. CMIP5 model data revealed a strong rise in the FLH until the end of this century. Even under the most optimistic scenario RCP2.6, the FLH may continue increasing (approximately 230 m ± 190 m) at a similar rate as in the last three decades. For the most pessimistic scenario RCP8.5, the rise in FLH is very large (approximately 875 m ± 390), being almost three times the observed warming in the last three decades. The surface area above the projected FLH under RCP2.6 is about half of the area above the present-day wet season FLH. The area above the RCP8.5 FLH is very small and consists only of the highest peaks in the region. This will certainly have severe impacts on the environment.
3. We found a relation of the present-day wet season FLHs from reanalysis data and regional-scale glacier extents, supported by the close relation between FLH, SLH, and glacier energy balance. Below the wet season FLH, annual glacier surface ablation is typically very high, thus exerting an important control on the glacier terminus especially for small and midsized glaciers. Based on this relation, even under the most optimistic scenario, at least half of the current glacier area will vanish by the end of this century. Under the most pessimistic scenario, not only small to midsized glaciers but also large glaciers may retreat within this century and only some patches of ice would remain on the summits of the highest peaks. Although we used a very simple experiment, we suggest that this is a robust and rather optimistic estimation for the future glacier extent. Of course, future glacier extents are related to large uncertainties, which are still difficult to quantify (e.g., changes in other climatic variables, glacier response times, and glacier geometries). The large difference between the most optimistic and pessimistic scenarios for the future of our climate and glacier extents, however, is not a result of model uncertainty but is a strong indicator of the differential effects of low-emission and high-emission scenarios on glaciers, and underlines the importance of strong greenhouse gas emission reduction policies. In upcoming research our estimates of present-day and future FLHs could be implemented in energy and mass balance models in order to estimate more accurately the future retreat of these glaciers, the timing, and the corresponding uncertainties.

Acknowledgments

This research was developed in the framework of Proyecto Glaciares+, a program financed by the Swiss Agency for Development and Cooperation SDC, in collaboration with CARE Peru. We acknowledge the use of data from the SENAMHI. Stations from the UNASAM were installed in the framework of the project Centro de Información e Investigación Ambiental de Desarrollo Regional Sostenible (CIIADERS). ERA-interim data are obtained from the ECMWF. The MERRA2 data are provided by the Global Modeling and Assimilation Office (GMAO) at NASA Goddard Space Flight Center. TRMM PR 2A23 and 2A25 data are obtained from the Japan Aerospace Exploration Agency (JAXA) and the National Aeronautics and Space Administration (NASA). GLIMS data are provided by the National Snow and Ice Data Center, and the ASTER DEM is obtained through the DAAC Global Data Explorer, a product of METI and NASA. Raphael Neukom is supported by the Swiss NSF grant PZ00P2_154802. J.L. Endries and L.B. Perry were supported by the U.S. National Science Foundation through grant AGS-1347179 (CAREER: Multiscale Investigations of Tropical Andean Precipitation). The authors are grateful to the editor and three anonymous reviewers for their invaluable and constructive suggestions and comments that helped improve the manuscript. The data supporting the analysis can be obtained by sending a written request to the corresponding authors (Simone Schauwecker, schauwecker@meteodat.ch).

References

American Meteorological Society (2016), Glossary of meteorology. [Available online at http://glossary.ametsoc.org/wiki/.]

Ames, A., and S. Hastenrath (1996), Diagnosing the imbalance of Glaciar Santa Rosa, Cordillera Raura, Peru, *J. Glaciol.*, *42*, 212–218.

Awaka, J., T. Iguchi, and K. Okamoto (2009), TRMM PR Standard Algorithm 2A23 and its performance on Bright Band detection, *J. Meteorol. Soc. Jpn.*, *87A*, 31–52.

Baraer, M., B. G. Mark, J. M. McKenzie, T. Condom, J. Bury, K.-I. Huh, C. Portocarrero, J. Gómez, and S. Rathay (2012), Glacier recession and water resources in Peru's Cordillera Blanca, *J. Glaciol.*, *58*, 134–150.

Battan, L. J. (1973), *Radar Observation of the Atmosphere*, p. 324, The Univ. of Chicago Press, Chicago.

Bosilovich, M. G., et al. (2015), *MERRA-2: Initial Evaluation of the Climate*, *Tech. Rep. Ser. on Global Model. and Data Assimilation*, vol. 43, Goddard Space Flight Center, Greenbelt, Md.

Bradley, R. S., F. T. Keimig, and H. F. Diaz (2004), Projected temperature changes along the American cordillera and the planned GCOS network, *Geophys. Res. Lett.*, *31*, L16210, doi:10.1029/2004GL020229.

Bradley, R. S., M. Vuille, H. F. Diaz, and W. Vergara (2006), Threats to water supplies in the tropical Andes, *Science*, *312*, 1755–1756.

Bradley, R. S., F. T. Keimig, H. F. Diaz, and D. R. Hardy (2009), Recent changes in freezing level heights in the tropics with implications for the deglacierization of high mountain regions, *Geophys. Res. Lett.*, *36*, L17701, doi:10.1029/2009GL037712.

Condom, T., A. Coudrain, J. E. Sicart, and S. Théry (2007), Computation of the space and time evolution of equilibrium-line altitudes on Andean glaciers (10°N–55°S), *Global Planet. Change*, *59*, 189–202.

Dee, D. P., et al. (2011), The ERA-Interim reanalysis: Configuration and performance of the data assimilation system, *Q. J. R. Meteorol. Soc.*, *137*, 553–597.

Diaz, H. F., J. K. Eischeid, C. Duncan, and R. S. Bradley (2003), Variability of freezing levels, melting season indicators, and snow cover for selected high-elevation and continental regions in the last 50 years, *Clim. Change*, *59*, 33–52.

Diaz, H. F., R. S. Bradley, and L. Ning (2014), Climatic changes in mountain regions of the American Cordillera and the tropics: Historical changes and future outlook, *Arct. Antarct. Alp. Res.*, *46*, 1–9.

Drenkhan, F., M. Carey, C. Huggel, J. Seidel, and M. T. Oré (2015), The changing water cycle: Climatic and socioeconomic drivers of water-related changes in the Andes of Peru, *Wiley Interdiscip. Rev. Water*, *2*, 715–733.

Favier, V., P. Wagnon, and P. Ribstein (2004a), Glaciers of the outer and inner tropics: A different behaviour but a common response to climatic forcing, *Geophys. Res. Lett.*, *31*, L16403, doi:10.1029/2004GL020654.

Favier, V., P. Wagnon, J.-P. Chazarin, L. Maisincho, and A. Coudrain (2004b), One-year measurements of surface heat budget on the ablation zone of Antizana Glacier 15, Ecuadorian Andes, *J. Geophys. Res.*, 109, D18105, doi:10.1029/2003JD004359.

Francou, B., M. Vuille, V. Favier, and B. Cáceres (2004), New evidence for an ENSO impact on low-latitude glaciers: Antizana 15, Andes of Ecuador, 0°28′S, *J. Geophys. Res.*, *109*, D18106, doi:10.1029/2003JD004484.

Garreaud, R. D., M. Vuille, and A. C. Clement (2003), The climate of the Altiplano: Observed current conditions and mechanisms of past changes, *Palaeogeogr. Palaeoclimatol. Palaeoecol.*, *194*, 5–22.

Global Land and Ice Measurements from Space and National Snow and Ice Data Center (2005), updated 2012) *GLIMS Glacier Database, Version 1*, NSIDC: Natl. Snow and Ice Data Cent., Boulder, Colo.

Guilyardi, E., H. Bellenger, M. Collins, S. Ferrett, W. Cai, and A. Wittenberg (2012), A first look at ENSO in CMIP5, *CLIVAR Exchanges*, *58*, 29–32.

Gurgiser, W., B. Marzeion, L. Nicholson, M. Ortner, and G. Kaser (2013a), Modeling energy and mass balance of Shallap Glacier, Peru, *Cryosphere*, *7*, 1787–1802.

Gurgiser, W., T. Mölg, L. Nicholson, and G. Kaser (2013b), Mass-balance model parameter transferability on a tropical glacier, *J. Glaciol.*, *59*, 845–858.

Gurgiser, W., I. Juen, K. Singer, M. Neuburger, S. Schauwecker, M. Hofer, and G. Kaser (2016), Comparing peasants' perceptions of precipiation change with precipiation records in the tropical Callejón de Huaylas, Peru, *Earth Syst. Dyn.*, *7*, 499–515.

Harris, G. N., K. P. Bowman, and D.-B. Shin (2000), Comparison of freezing-level altitudes from the NCEP reanalysis with TRMM precipitation radar Brightband data, *J. Clim.*, *13*, 4137–4148.

Hofer, M., T. Mölg, B. Marzeion, and G. Kaser (2010), Empirical-statistical downscaling of reanalysis data to high-resolution air temperature and specific humidity above a glacier surface (Cordillera Blanca, Peru), *J. Geophys. Res.*, *115*, D12120, doi:10.1029/2009JD012556.

Intergovernmental Panel on Climate Change (IPCC) (2000), *Special Report on Emission Scenarios*, p. 570, Cambridge Univ. Press, U. K.

Intergovernmental Panel on Climate Change (IPCC) (2013), *Climate Change 2013: The Physical Science Basis. Contribution of Working Group I to the Fifth Assessment Report of the Intergovernmental Panel on Climate Change*, edited by T. F. Stocker et al., pp. 1045–1047, Cambridge Univ. Press, Cambridge, U. K., and New York.

Juen, I., G. Kaser, and C. Georges (2007), Modelling observed and future runoff from a glacierized tropical catchment (Cordillera Blanca, Perú), *Global Planet. Change*, *59*, 37–48.

Kaser, G. (2001), Glacier-climate interaction at low latitudes, *J. Glaciol.*, *47*, 195–204.

Kaser, G., A. Ames, and M. Zamora (1990), Glacier fluctuations and climate in the Cordillera Blanca, Peru, *Ann. Glaciol.*, *14*, 136–140.

Kaser, G., and C. Georges (1997), Changes of the equilibrium-line altitude in the tropical Cordillera Blanca, Peru, 1930–50, and their spatial variations, *Ann. Glaciol.*, *24*, 344–349.

Kaser, G., and H. Osmaston (2002), *Tropical Glaciers*, p. 35, Cambridge Univ. Press, Cambridge.

Kaser, G., I. Juen, C. Georges, J. Gómez, and W. Tamayo (2003), The impact of glaciers on the runoff and the reconstruction of mass balance history from hydrological data in the tropical Cordillera Blanca, Peru, *J. Hydrol.*, *282*, 130–144.

Kaser, G., M. Grosshauser, and B. Marzeion (2010), Contribution potential of glaciers to water availability in different climate regimes, *Proc. Natl. Acad. Sci. U.S.A.*, *107*, 20,223–20,227.

Klok, E. J., and J. Oerlemans (2002), Model study of the spatial distribution of the energy and mass balance of Morteratschgletscher, Switzerland, *J. Glaciol.*, *48*, 505–518.

López-Moreno, J. I., S. Fontaneda, J. Bazo, J. Revuelto, C. Azorin-Molina, B. Valero-Garcés, E. Morán-Tejeda, S. M. Vicente-Serrano, R. Zubieta, and J. Alejo-Cochachín (2014), Recent glacier retreat and climate trends in Cordillera Huaytapallana, Peru, *Global Planet. Change*, *112*, 1–11.

Lynch, B. (2012), Vulnerabilities, competition and rights in a context of climate change toward equitable water governance in Peru's Rio Santa Valley, *Global Environ. Change*, *22*, 364–373.

Mark, B. G., and G. O. Seltzer (2003), Tropical glacier meltwater contribution to stream discharge: A case study in the Cordillera Blanca, Peru, *J. Glaciol.*, *49*, 271–281.

Mark, B. G., and G. O. Seltzer (2005), Evaluation of recent glacier recession in the Cordillera Blanca, Peru (AD 1962–1999): Spatial distribution of mass loss and climatic forcing, *Quat. Sci. Rev.*, *24*, 2265–2280.
Mark, B. G., J. M. McKenzie, and J. Gómez (2005), Hydrochemical evaluation of changing glacier meltwater contribution to stream discharge: Callejon de Huaylas, Peru, *Hydrol. Sci. J.*, *50*, 975–987.
Maussion, F., W. Gurgiser, M. Grosshauser, G. Kaser, and B. Marzeion (2015), ENSO influence on surface energy and mass balance at Shallap Glacier, Cordillera Blanca, Peru, *Cryosphere*, *9*, 1663–1683.
Minveille, M., and R. D. Garreaud (2011), Projecting rainfall changes over the South American Altiplano, *J. Clim.*, *24*, 4577–4583.
Moss, R. H., et al. (2010), The next generation of scenarios for climate change research and assessment, *Nature*, *463*, 747–756.
NASA Jet Propulsion Laboratory (2009), *ASTER Global Digital Elevation Model*, NASA JPL, doi:10.5067/ASTER/ASTGTM.002.
National Oceanic and Atmospheric Administration (2016), ftp://tgftp.nws.noaa.gov/data/observations/metar, last access: 1 May 2016.
Neukom, R., M. Rohrer, P. Calanca, N. Salzmann, C. Huggel, D. Acuña, D. A. Christie, and M. S. Morales (2015), Facing unprecedented drying of the Central Andes? Precipitation variability over the period AD 1000–2100, *Environ. Res. Lett.*, *10*, 84017.
Perry, L. B., et al. (2017), Characteristics of precipitation storms in glacierized tropical Andean Cordilleras of Peru and Bolivia, *Ann. Assoc. Am. Geogr.*, *107*, 309–322.
Poremba, R. J., L. B. Perry, A. Semon, D. T. Martin, and A. Tupayachi (2015), Meteorological characteristics of heavy snowfall in the Cordillera Vilcanota, Peru. 72nd Eastern Snow Conf., Sherbrooke, Québec, Canada.
Prinz, R., L. I. Nicholson, T. Mölg, W. Gurgiser, and G. Kaser (2016), Climatic controls and climate proxy potential of Lewis Glacier, Mt. Kenya, *Cryosphere*, *10*, 133–148.
Rabatel, A., A. Bermejo, E. Loarte, A. Soruco, J. Gomez, G. Leonardini, C. Vincent, and J. E. Sicart (2012), Can the snowline be used as an indicator of the equilibrium line and mass balance for glaciers in the outer tropics?, *J. Glaciol.*, *58*, 1027–1036.
Rabatel, A., et al. (2013), Current state of glaciers in the tropical Andes: A multicentury perspective on glacier evolution and climate change, *Cryosphere*, *7*, 81–102.
Racoviteanu, A. E., Y. Arnaud, M. W. Williams, and J. Ordonez (2008), Decadal changes in glacier parameters in the Cordillera Blanca, Peru, derived from remote sensing, *J. Glaciol.*, *54*, 499–510.
Rienecker, M. M., et al. (2011), MERRA2: NASA's modern-era retrospective analysis for research and applications, *J. Clim.*, *24*, 3624–3648.
Sagredo, E. A., S. Rupper, and T. V. Lowell (2014), Sensitivities of the equilibrium line altitude to temperature and precipitation changes along the Andes, *Quat. Res.*, *81*, 355–366.
Salzmann, N., C. Huggel, M. Rohrer, W. Silverio, B. G. Mark, P. Burns, and C. Portocarrero (2013), Glacier changes and climate trends derived from multiple sources in the data scarce Cordillera Vilcanota region, southern Peruvian Andes, *Cryosphere*, *7*, 103–118.
Schauwecker, S., et al. (2014), Climate trends and glacier retreat in the cordillera Blanca, Peru, revisited, *Global Planet. Change*, *119*, 85–97.
Schauwecker, S., M. Rohrer, M. Schwarb, C. Huggel, A. P. Dimri, and N. Salzmann (2016), Estimation of snowfall limit for the Kashmir Valley, Indian Himalayas, with TRMM PR Bright Band information, *Meteorol. Z.*, *25*, 501–509.
Tan, I., T. Storelvmo, and M. D. Zelinka (2016), Observational constraints on mixed-phase clouds imply higher climate sensitivity, *Science*, *352*, 224–227.
Taylor, K. E., R. J. Stouffer, and G. A. Meehl (2011), An overview of CMIP5 and the experiment design, *Bull. Am. Meteorol. Soc.*, *93*, 485–498.
Thurai, M., E. Deguchi, T. Iguchi, and K. Okamoto (2003), Freezing height distribution in the tropics, *Int. J. Satell. Commun. Netw.*, *21*, 533–545.
Urrutia, R., and M. Vuille (2009), Climate change projections for the tropical Andes using a regional climate model: Temperature and precipitation simulations for the end of the 21st century, *J. Geophys. Res.*, *114*, D02108, doi:10.1029/2008JD011021.
Viste, E., and A. Sorteberg (2015), Snowfall in the Himalayas: An uncertain future from a little-known past, *Cryosphere*, *9*, 1147–1167.
Vuille, M., and R. S. Bradley (2000), Mean annual trends and their vertical structure in the tropical Andes, *Geophys. Res. Lett.*, *27*, 3885–3888, doi:10.1029/2000GL011871.
Vuille, M., B. Francou, P. Wagnon, I. Juen, G. Kaser, B. G. Mark, and R. S. Bradley (2008), Climate change and tropical Andean glaciers: Past, present and future, *Earth Sci. Rev.*, *89*, 79–96.
Wang, S., M. Zhang, N. C. Pepin, Z. Li, M. Sun, X. Huang, and Q. Wang (2014), Recent changes in freezing level heights in High asia and their impacts on glacier changes, *J. Geophys. Res. Atmos.*, *119*, 1753–1765.
Zemp, M., et al. (2015), Historically unprecedented global glacier decline in the early 21st century, *J. Glaciol.*, *61*, 745–761.